SCIENTIFIC REPORTS

OPEN

Strain induced piezoelectric effect in black phosphorus and MoS_2 van der Waals heterostructure

Received: 01 July 2015
Accepted: 14 October 2015
Published: 10 November 2015

Le Huang, Yan Li, Zhongming Wei & Jingbo Li

The structural, electronic, transport and optical properties of black phosphorus/MoS_2 (BP/MoS_2) van der Waals (vdw) heterostructure are investigated by using first principles calculations. The band gap of BP/MoS_2 bilayer decreases with the applied normal compressive strain and a semiconductor-to-metal transition is observed when the applied strain is more than 0.85 Å. BP/MoS_2 bilayer also exhibits modulation of its carrier effective mass and carrier concentration by the applied compressive strain, suggesting that mobility engineering and good piezoelectric effect can be realized in BP/MoS_2 heterostructure. Because the type-II band alignment can facilitate the separation of photo-excited electrons and holes, and it can benefit from the great absorption coefficient in ultra-violet region, the BP/MoS_2 shows great potential to be a very efficient ultra-violet photodetector.

Despite being a very promising two-dimensional (2D) material, gapless graphene has limitation in its applications in nanoelectronics and optoelectronics[1–3]. As alternatives, new researches have emerged focusing on other 2D materials such as transition metal sulfides (TMDs), which possess sizable band gap and display advantageous optoelectronic properties[4–7]. For example, bulk MoX_2 (X = S, Se, Te) and WX_2 are indirect band gap semiconductors, whereas their monolayers have direct band gaps, which are favorable for optoelectronic applications. The single-layer MoS_2 based field-effect transistors exhibit an excellent current on/off ratio of 10^8[8], and the application of monolayer MoS_2 in integrated circuits and logic operations has already been realized[9].

Recently, a new 2D layered material, namely black phosphorus (BP) has been fabricated by several research groups[10–12]. Similar to other 2D materials, different BP layers binding together via the weak van der Waals (vdW) force. Theoretical calculations show that the band gap of BP is layer dependent with 0.30 eV in bulk BP and 0.90 eV in its monolayer form[12–15]. What's more, bulk BP shows a high hole mobility up to 10000 cm^2/Vs[16]. And well-behaved p-type field-effect transistors with mobilities of up to 1000 cm^2/Vs have been demonstrated on few-layer BP[10]. These properties make BP a potential candidate for novel applications in nanoelectronics and optoelectronics.

Recent studies have shown that hybrid systems consisting of various 2D materials would provide more opportunities for achieving desired electronic and optoelectronic properties[17–21]. For example, remarkable multiple optoelectronic functionality, including highly sensitive photodetection and gate-tunable persistent photoconductivity has been observed in the graphene/MoS_2 vdW heterostructures[22]. The vertical field-effect transistors based on the graphene-WS_2 heterostructures are also fabricated with unprecedented current modulation exceeding 10^6 at room temperature[23]. Moreover, Yexin Deng *etc* demonstrated that a gate-tunable p-n diode based on a p-type BP/n-type monolayer MoS_2 vdw p-n heterojunction shows a maximum photodetection responsivity of 418 mA/W at the wavelength of 633 nm[24]. An anomalous photoluminescence quenching is observed in artificial heterostacks of monolayer TMDs and few-layer BP[25]. J. E. Padilha *etc* reported that the Schottky barrier height and doping of phosphorus can be controlled by applying an external perpendicular electric field[26].

State Key Laboratory for Superlattice and Microstructures, Institute of Semiconductors, Chinese Academy of Sciences, Beijing 100083, China. Correspondence and requests for materials should be addressed to Z.W. (email: zmwei@semi.ac.cn) or J.L. (email: jbli@semi.ac.cn)

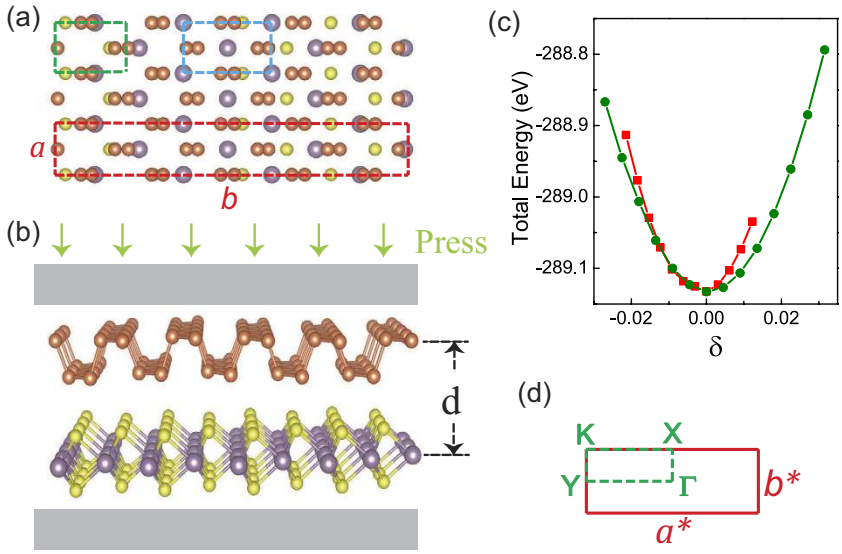

Figure 1. (**a**) Top view and (**b**) side view of BP/MoS_2 bilayer. The green and blue rectangular regions present the unit cells of BP and MoS_2. The supercell of BP/MoS_2 bilayer is depicted in red rectangular region. (**c**) Evolution of the total energy of BP/MoS_2 bilayer as a function of uniaxial strains. (**d**) Brillouin zone with high-symmetry points labeled.

In this work, we investigate the effect of normal compressive strain on the structural, electronic, transport and optical properties of semiconducting BP/MoS_2 vdW heterostructure. The band gap of BP/MoS_2 decreases with the applied strain and a semiconductor-to-metal transition is observed when the applied compressive strain is more than 0.85 Å. The compressive strain also exerts influence on the charge carrier effective mass and concentration, suggesting that mobility engineering and good piezoelectric effect can be realized in BP/MoS_2 heterostructure. The calculated optical property of BP/MoS_2 shows that BP/MoS_2 may be a very efficient ultra-violet photodetector because the type-II band alignment can facilitate the separation of photo-excited electrons and holes, and it can benefit from the great absorption coefficient in ultra-violet region.

Results and Discussion

Top and side views of the relaxed atomic structure of BP/MoS_2 bilayer are shown in Fig. 1. To minimize the lattice mismatch between the stacking sheets, a rectangular unit cell of MoS_2 is constructed. The supercell of this system is composed by 1×4 unit cells of BP and 1×5 unit cells of MoS_2, which is the same with our previous work[27]. The optimised lattice constants of monolayer MoS_2 are $a_M = 3.19$ Å, $b_M = 5.53$ Å and the calculated lattice constants of monolayer BP are $a_P = 3.30$ Å, $b_P = 4.62$ Å. To determine the stable structure of BP/MoS_2 bilayer, the total energy as a function of uniaxial strains along X (zigzag) and Y (armchair) directions is depicted in Fig. 1(c). Both curves show their minimas under zero strain, at which point, the lattice constants of the supercell employed here are $a = 3.26$ Å, $b = 22.18$ Å.

Tuning the band gaps of 2D materials has been a challenge in band gap engineering. Many techniques, such as in-plane strains[28–31] and a strong external electric field[32,33], are promising but suffer from lack of practical applicability. Therefore, in this work, the effect of applied normal compressive strain on the electronic and optical properties of BP/MoS_2 is studied. The strain is calculated as $\varepsilon = d_0 - d$, where d_0 and d are the equilibrium and instantaneous distances between the top phosphorus atom layer and the molybdenum atom layer. In Fig. 2, we show the projected band structure of BP/MoS_2 bilayer under different compressive strain. Figure 1(d) presents the Brillouin zone of rectangular cells with high-symmetry points labeled. In Fig. 2, the bands dominated by BP and MoS_2 are plotted by blue red dots, respectively. It is clear that the conduction band minimum (CBM) and the valence band maximum (VBM) are dominated by MoS_2 and BP, respectively, regardless of the applied compressive strain. More importantly, BP/MoS_2 vdW heterostructure has a type-II band alignment and thus the lowest energy electron-hole pairs are spatially separated with electrons and holes locating in MoS_2 and BP layer, respectively. These results indicate that BP/MoS_2 vdW heterostructure may be suitable for optoelectronics and solar energy conversion.

Evolution of band edges and total energy of BP/MoS_2 bilayer as a function of the applied compressive strain is concluded in Fig. 3(a). It can be proved that the interlayer distance d_0 at equilibrium state is 6.92 Å. The vdW interaction exerts little influence on the band edges of BP/MoS_2. The BP/MoS_2 bilayer shows a finite indirect band gap up to 0.45 eV. Upon applying compressive strain, both the VBM and CBM move towards the Fermi level, resulting in a decreasing band gap with the applied strain.

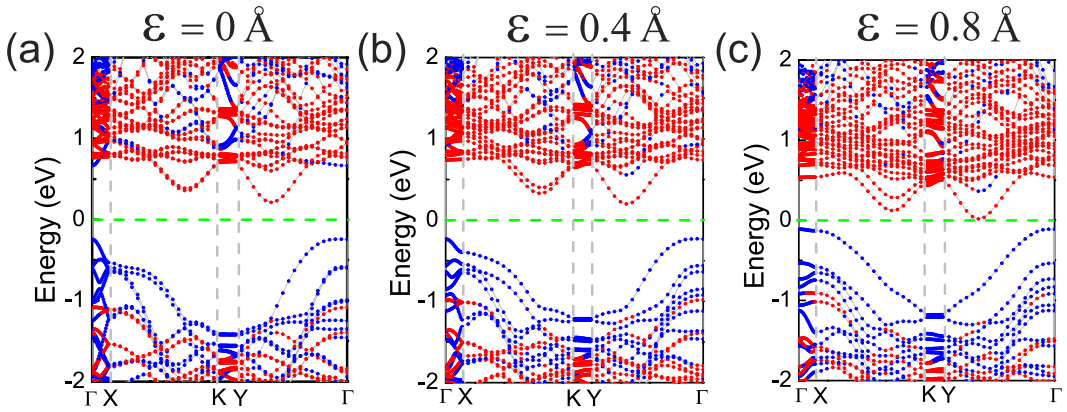

Figure 2. Evolution of projected band structure of BP/MoS_2 bilayer as a function of the applied compressive strain. The bands dominated by BP and MoS_2 are plotted by blue red dots, respectively.

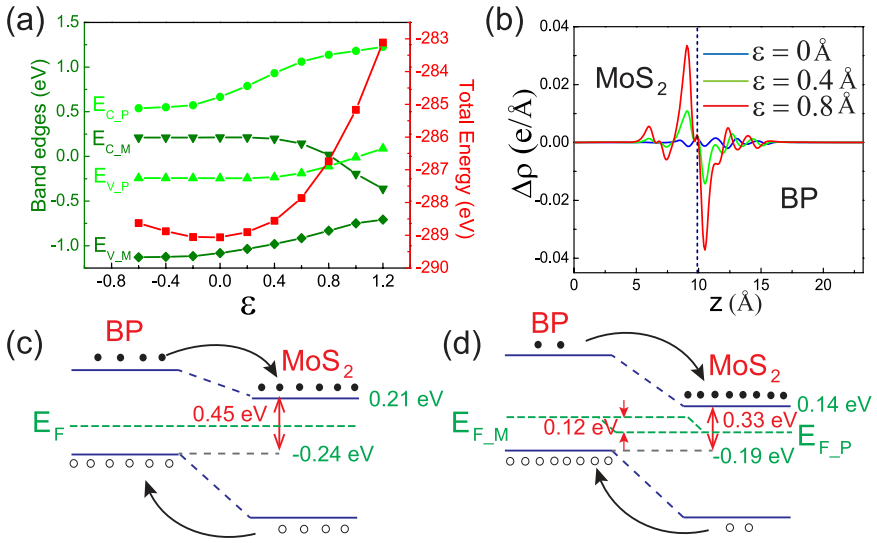

Figure 3. (**a**) Evolution of band edges and total energy of BP/MoS_2 bilayer as a function of the applied compressive strain. (**b**) The difference between the integrated charge density of BP/MoS_2 bilayer under different compressive strain and that of the isolated monolayers. (**c**,**d**) The band alignment of BP/MoS_2 bilayer under applied compressive strain of 0 Å and 0.4 Å, respectively. $E_{F\_P(M)}$ is the quasi-fermi level of BP (MoS_2) in BP/MoS_2 bilayer.

The BP/MoS_2 bilayer experiences a semiconductor-to-metal transition when the applied compressive strain is larger than 0.85 Å, which may lead to tunable conductivity and transport properties.

The difference between the integrated charge density of BP/MoS_2 bilayer under different compressive strain and that of the isolated monolayers as a function of the perpendicular distance is shown in Fig. 3(b). It is calculated as

$$\Delta\rho(z) = \int \rho_S(x, y, z)\,dxdy - \int \rho_{BP}(x, y, z)\,dxdy - \int \rho_{MoS_2}(x, y, z)\,dxdy$$

where $\rho_s(x,y,z)$, $\rho_{BP}(x,y,z)$ and $\rho_{MoS_2}(x, y, z)$ are the charge density at the (x, y, z) point in BP/MoS_2 supercell, BP and MoS_2 monolayer supercell, respectively. It is found that there is a small amount of charge exchange between BP layer to MoS_2 layer. Furthermore, the applied compressive strain can facilitate electrons transferring from BP to MoS_2 layer and holes transferring from MoS_2 to BP layer. More charge transfer between BP layer and MoS_2 layer suggests an increased carrier concentration and a stronger interlayer interaction. When under compressive strain, the quasi-fermi level of MoS_2 moves upward and the quasi-fermi level of BP layer moves downward, as shown in Fig. 3(c,d). As a result, the band gap of BP/MoS_2 bilayer decreases with the applied compressive strain.

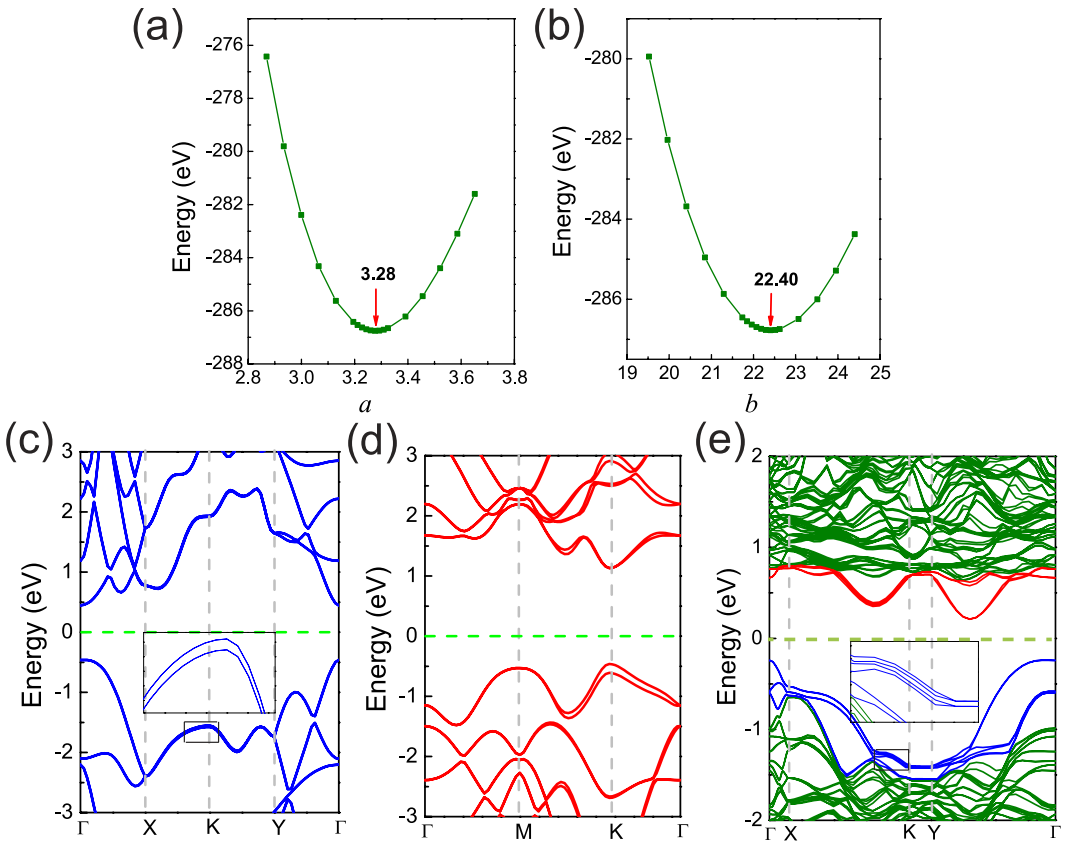

Figure 4. (**a**,**b**)The variation of the total energy with planar lattice constant, *a* and *b*, in BP/MoS_2 bilayer under a normal compressive stran of 0.8 Å. The band structures of BP monolayer, MoS_2 monolayer and BP/MoS_2 heterostructure, including SOC effect are shown in (**c**–**e**) respectively.

For a three-dimensional material, when it is compressed along z direction, it usually will expand in the planar x and y directions. This effect is also taken into consideration in this work. Figure 4(a,b) gives the variation of the total energy with planar lattice constant, *a* and *b*, in BP/MoS_2 bilayer under a normal compressive stran of 0.8 Å. It is found that the total energy reaches its minima when $a = 3.28$ Å, $b = 22.40$ Å, respectively. Both *a* and *b* are a little larger than that of BP/MoS_2 bilayer without strains. It can be concluded that for the BP/MoS_2 heterostructure, when exerting compressive strain along z direction, it also will expand in the planar x and y direction, just as a three-dimensional material.

Monolayer MoS_2 has been reported to have a intrinsic spin-orbit gap. Whether the spin-orbit coupling (SOC) effect will exert obvious influence on the band gap of BP/MoS_2 heterostructure is unknown. In Fig. 4(c,d), the band structures of BP and MoS_2 monolayer, including SOC effect, are shown. BP and MoS_2 monolayer show a spin-orbit gap of 22 meV and 147 meV at K point in the valence band, which are in good agreement with previous works[15,34]. As shown in Fig. 4(e), though the SOC gap of MoS_2 can be comparable to the band gap of the BP/MoS_2 heterostructure under compressive strain, the SOC exerts little influence on the band gap of BP/MoS_2 because the VBM in the band structure of BP/MoS_2 bilayer is dominated by BP whose SOC gap is very small rather than by MoS_2. So the SOC effect is not taken into consideration in following results.

With the applied normal compressive strain exerting influence on the band structure of BP/MoS_2 bilayer, a change in the effective masses of electrons and holes can be expected. Figure 5 displays the changes of electron and hole effective masses with the compressive strain. The effective mass is calculated using $m = \hbar^2/(\partial^2 E/\partial k^2)$, and the *k* points closely approach the VBM and CBM. In the band structure of BP/MoS_2 bilayer, it is clear that the CBM is located at a point between Y and Γ. The curve labeled CBM[Y] shows the effective mass of electron at CBM along Y direction. The electron effective mass (m_e) at CBM in the Γ direction is much smaller than that in the Y direction and it decreases gradually with applied compressive strain. The hole effective mass (m_h) at Γ is quite sensitive to the compressive strain. m_h in the X direction increases drastically in the case of compressive strain larger than 0.4 Å, while that in the Y direction decreases gradually with the compressive strain. It also can be seen that the minimum of both m_e and m_h is much smaller than 1, suggesting that BP/MoS_2 as a type-II heterostructure may possesses great transport properties such as high mobility and conductivity. BP/MoS_2 vdW heterostructure may have great potential for applications in nanoelectronics and optoelectronics.

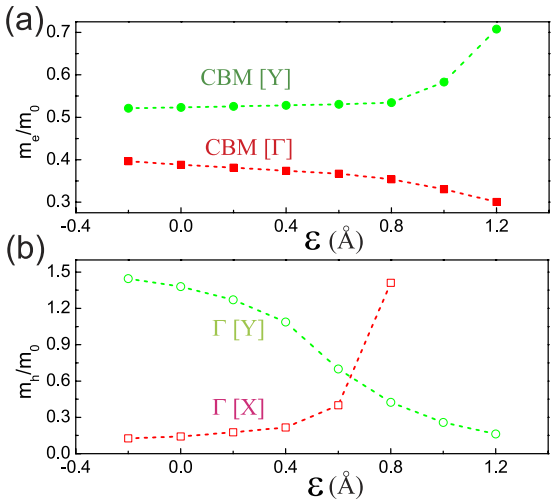

Figure 5. Effective masses (in units of electron mass m0) of (**a**) electrons and (**b**) holes as a function of applied compressive strain. The masses are labeled by the band extremum and the direction (in square brackets) along which the mass is calculated. The vertical dashed line indicates unstrained BP/MoS_2.

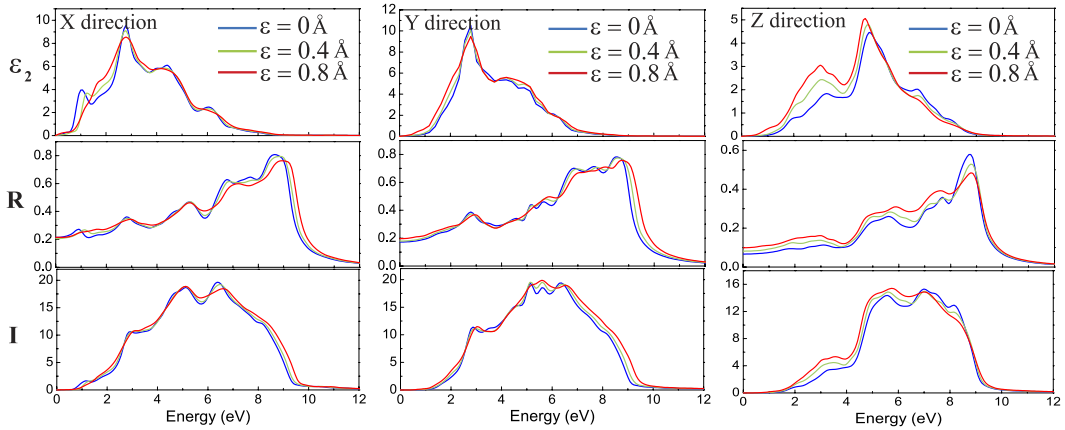

Figure 6. Calculated optical properties in (**a**) X directin, (**b**) Y direction and (**c**) perpendicular direction of BP/MoS2 bilayer under different compressive strain. From top to bottom planets are imaginary part of the dielectric function ε_2, reflectivity R and absorption coefficient I, respectively.

Very recently, it is predicted that the BP/TMD system is a more efficient solar cell than the graphene/TMD systems[35–37] because the former can benefit from the absorption of wider range of wavelength in the solar spectrum, and the type-II heterojunction alignment can allow more efficient hole-electron separation. In Fig. 6, therefore, the real (ε_1) and imaginary (ε_2) parts of the frequency-dependent dielectric functions are calculated by GGA-PBE and the frequency-dependent reflectivity R and absorption coefficient I are computed. Different with hexagonal lattice, the dielectric tensor has three independent components, namely, ε^X, ε^Y and $\varepsilon^\perp$. Strong anisotropy is observed in the imaginary parts of dielectric functions ε_2^X, ε_2^Y and $\varepsilon_2^\perp$. The variations of reflectivity and absorption coefficients as the function of frequency also exhibit similar trend, as illustrated in middle and bottom planets. From the absorption spectrum (the bottom planet), we can find that BP/MoS_2 bilayer may have good application in ultraviolet light (above 3.27 eV) detecting. Furthermore, the effect of applied normal compressive strain on the optical properties of BP/MoS_2 bilayer is also studied. The applied compressive strain shows little influence on the optical properties in the X and Y directions, while exerts much more remarkable influence on the three optical parameters in perpendicular direction ($\varepsilon_2^\perp$, $R^\perp$ and $I^\perp$). It is because the compressive strain just enhances the interlayer interaction while exerts no influence on the in-plane interaction.

Conclusion

In summary, we have provided total energy and band structure calculations for the p-type BP/n-type MoS_2 vdW heterostructure and investigated its structural, electronic, transport and optical properties

by using first principles calculations. The decreased band gap by applied compressive strain indicates the great application potential of BP/MoS_2 vdW heterostructures in future nanoelectronics such as field effect transistors. A semiconductor-to-metal transition can be observed in BP/MoS_2 bilayer under the compressive strain. The reduced carrier effective mass and improved carrier concentration by the applied compressive strain suggest that mobility engineering and good piezoelectric effect can be realized in BP/MoS_2 bilayer. Furthermore, because the type-II heterojunction alignment can facilitate the separation of photo-excited electrons and holes, and it can benefit from the great absorption coefficient in ultra-violet region the BP/MoS_2 heterostructure may be a very efficient ultra-violet photodetector. According to our results, the BP/MoS_2 vdw p-n heterojuntion will present abundant opportunities for application in future nano- and optoelectronics such as photovoltaic cell, photodetector and logical device.

Methods

The first-principles calculations are performed by VASP code within plane-wave basis sets and Perdew-Burke-Ernzerhof (PBE) projector augmented wave pseudopotentials[38–40]. The semi-empirical DFT-D2 method method of Grimme is utilized for the dispersion correction in the interlayer interaction[41]. The plane-wave cutoff energy is set to be 500 eV and a vacuum larger than 12 Å is used to simulate the isolated sheet. The first Brillouin zone is sampled with a $(15 \times 15 \times 1)$ Monkhorst-Pack grid for relaxation of BP and MoS_2 unitcells[42]. A $(5 \times 20 \times 1)$ Monkhorst-Pack grid is used for relaxation of supercells. All the structures are fully relaxed with a force tolerance of 0.01 eV/Å.

References

1. Geim, A. K. Graphene: status and prospects. *Science* **324,** 1530–1534 (2009).
2. Avouris, P., Chen, Z. & Perebeinos, V. Carbon-based electronics. *Nat. Nanotechnol.* **2,** 605–615 (2007).
3. Schwierz, F. Graphene transistors. *Nat. Nanotechnol.* **5,** 487–496 (2010).
4. Tsai, D.-S. *et al.* Few-layer MoS_2 with high broadband photogain and fast optical switching for use in harsh environments. *ACS Nano* **7,** 3905–3911 (2013).
5. Lopez-Sanchez, O. *et al.* Ultrasensitive photodetectors based on monolayer MoS_2. *Nat. Nanotechnol.* **8,** 497–501 (2013).
6. Coleman, J. N. *et al.* Two-dimensional nanosheets produced by liquid exfoliation of layered materials. *Science* **331,** 568–571 (2011).
7. Korn, T. *et al.* Low-temperature photocarrier dynamics in monolayer MoS_2. *Appl. Phys. Lett.* **99,** 102109 (2011).
8. Radisavljevic, B. *et al.* Single-layer MoS_2 transistors. *Nat. Nanotechnol.* **6,** 147–150 (2011).
9. Radisavljevic, B., Whitwick, M. B. & Kis, A. Integrated circuits and logic operations based on single-layer MoS_2. *ACS Nano* **5,** 9934–9938 (2011).
10. Li, L. *et al.* Black phosphorus field-effect transistors. *Nat. Nanotechnol.* **9,** 372–377 (2014).
11. Castellanos-Gomez, A. *et al.* Isolation and characterization of few-layer black phosphorus. *2D Mater.* **1,** 025001 (2014).
12. Liu, H. *et al.* Phosphorene: an unexplored 2D semiconductor with a high hole mobility. *ACS Nano* **8,** 4033–4041 (2014).
13. Yan Li, S. Y. & Li, J. Modulation of the electronic properties of ultrathin black phosphorus by strain and electrical field. *J. Phys. Chem. C* **118,** 23970–23976 (2014).
14. Tran, V., Soklaski, R., Liang, Y. & Yang, L. Layer-controlled band gap and anisotropic excitons in few-layer black phosphorus. *Phys. Rev. B* **89,** 235319 (2014).
15. Rudenko, A. N. & Katsnelson, M. I. Quasiparticle band structure and tight-binding model for single-and bilayer black phosphorus. *Phys. Rev. B* **89,** 201408 (2014).
16. Morita, A. Semiconducting black phosphorus. *Appl. Phys. A:Solids Surf.* **39,** 227–242 (1986).
17. Peng, X. & Ahuja, R. Symmetry breaking induced bandgap in epitaxial graphene layers on SiC. *Nano Lett.* **8,** 4464–4468 (2008).
18. Britnell, L. *et al.* Field-effect tunneling transistor based on vertical graphene heterostructures. *Science* **335,** 947–950 (2012).
19. Behera, H. & Mukhopadhyay, G. Strain-tunable band gap in graphene/h-BN hetero-bilayer. *J. Phys. Chemi. Solids* **73,** 818–821 (2012).
20. Bertolazzi, S., Krasnozhon, D. & Kis, A. Nonvolatile memory cells based on MoS_2/graphene heterostructures. *ACS Nano* **7,** 3246–3252 (2013).
21. Balu, R., Zhong, X., Pandey, R. & Karna, S. P. Effect of electric field on the band structure of graphene/boron nitride and boron nitride/boron nitride bilayers. *Appl. Phys. Lett.* **100,** 052104 (2012).
22. Roy, K. *et al.* Graphene-MoS_2 hybrid structures for multifunctional photoresponsive memory devices. *Nature Nanotechnol.* **8,** 826–830 (2013).
23. Georgiou, T. *et al.* Vertical field-effect transistor based on graphene-WS_2 heterostructures for flexible and transparent electronics. *Nature Nanotechnol.* **8,** 100–103 (2013).
24. Deng, Y. *et al.* Black phosphorus–monolayer MoS_2 van der waals heterojunction p–n diode. *ACS Nano* **8,** 8292–8299 (2014).
25. Yuan, J. *et al.* Photoluminescence quenching and charge transfer in artificial hetero-stacks of monolayer transition metal dichalcogenides and few-layer black phosphorus. *ACS Nano* **9,** 555–563 (2015).
26. Padilha, J., Fazzio, A. & da Silva, A. J. Van der waals heterostructure of phosphorene and graphene: Tuning the schottky barrier and doping by electrostatic gating. *Phys. Rev. Lett.* **114,** 066803 (2015).
27. Le, H. *et al.* Electric-field tunable band offsets in black phosphorus and MoS_2 van der Waals p-n heterostructure. *J. Phys. Chem. Lett.* **6,** 2483–2488 (2015).
28. Scalise, E. *et al.* Strain-induced semiconductor to metal transition in the two-dimensional honeycomb structure of MoS_2. *Nano Res.* **5,** 43–48 (2012).
29. Han, X. *et al.* Strain and orientation modulated bandgaps and effective masses of phosphorene nanoribbons. *Nano Lett.* **14,** 4607–4614 (2014).
30. Fei, R. & Yang, L. Strain-engineering the anisotropic electrical conductance of few-layer black phosphorus. *Nano Lett.* **14,** 2884–2889 (2014).
31. Peng, X., Wei, Q. & Copple, A. Strain-engineered direct-indirect band gap transition and its mechanism in two-dimensional phosphorene. *Phys. Rev. B* **90,** 085402 (2014).
32. Ramasubramaniam, A., Naveh, D. & Towe, E. Tunable band gaps in bilayer transition-metal dichalcogenides. *Phys. Rev. B* **84,** 205325 (2011).
33. Das, S. *et al.* Tunable transport gap in phosphorene. *Nano Lett.* **14,** 5733–5739 (2014).
34. Cheiwchanchamnangi, T. & Lambrecht, W. Quasiparticle band structure calculation of monolayer, bilayer, and bulk MoS_2. *Phys. Rev. B* **85,** 205302 (2012).

35. Bernardi, M., Palummo, M. & Grossman, J. C. Extraordinary sunlight absorption and one nanometer thick photovoltaics using two-dimensional monolayer materials. *Nano Lett.* **13,** 3664–3670 (2013).
36. Britnell, L. *et al.* Strong light-matter interactions in heterostructures of atomically thin films. *Science* **340,** 1311–1314 (2013).
37. Guo, H. *et al.* Phosphorene nanoribbons, phosphorus nanotubes, and van der waals multilayers. *J. Phys. Chem. C* **118,** 14051–14059 (2014).
38. Blöchl, P. E. Projector augmented-wave method. *Phys. Rev. B* **50,** 17953 (1994).
39. Kresse, G. & Furthmuller, J. Efficient iterative schemes for ab initio total-energy calculations using a plane-wave basis set. *Phys. Rev. B* **54,** 11169 (1996).
40. Perdew, P., Burke, K. & Ernzerhof, M. Generalized gradient approximation made simple. *Phys. Rev. Lett.* **77,** 3865 (1996).
41. Grimme, S. Semiempirical gga-type density functional constructed with a long-range dispersion correction. *J. Comput. Chem.* **27,** 1787–1799 (2006).
42. Monkhorst, H. J. & Pack, J. D. Special points for brillouin-zone integrations. *Phys. Rev. B* **13,** 5188–5192 (1976).

Acknowledgements

This work was supported by the National Natural Science Foundation of China under Grant No. 91233120 and the National Basic Research Program of China (2011CB921901). Jingbo Li thankfully acknowledge financial support from the CAS/SAFEA International Partnership Program for Creative Research Teams. Zhongming Wei acknowledges financial support from the "Hundred Talents Program" of Chinese Academy of Sciences.

Author Contributions

Every author has made contribution to the manuscript. L.H. performed the density functional theory calculations. L.H. and Y.L. wrote the manuscript. Z.W. and J.L. guide the work.

Additional Information

Competing financial interests: The authors declare no competing financial interests.

How to cite this article: Huang, L. *et al.* Strain induced piezoelectric effect in black phosphorus and MoS_2 van der Waals heterostructure. *Sci. Rep.* **5**, 16448; doi: 10.1038/srep16448 (2015).